Copyright © 2013 American Scientific Publishers
All rights reserved
Printed in the United States of America

Journal of Nanoscience and Nanotechnology
Vol. 13, 6020–6026, 2013

RESEARCH ARTICLE

Fabrication of Biomolecules Self-Assembled on Au Nanodot Array for Bioelectronic Device

Taek Lee[1,2], Ajay Yagati Kumar[3], Si-Youl Yoo[1], Mi Jung[3], Junhong Min[4,*], and Jeong-Woo Choi[1,2,*]

[1] *Department of Chemical and Biomolecular Engineering, Sogang University, 35 Baekbeom-ro (Sinsu-dong), Mapo-gu, Seoul 121-742, Republic of Korea*
[2] *Research Institute for Basic Science, Sogang University, 35 Baekbeom-ro (Sinsu-dong), Mapo-gu, Seoul 121-742, Republic of Korea*
[3] *Interdisciplinary Program of Integrated Biotechnology, Sogang University, 35 Baekbeom-ro (Sinsu-dong), Mapo-gu, Seoul 121-742, Republic of Korea*
[4] *School of Integrative Engineering, Chung-Ang University, Heukseok-dong, Dongjak-gu, Seoul 156-756, Republic of Korea*

In the present study, an nano-platform composed of Au nanodot arrays on which biomolecules could be self-assembled was developed and investigated for a stable bioelectronic device platform. Au nanodot pattern was fabricated using a nanoporous alumina template. Two different biomolecules, a cytochrome c and a single strand DNA (ssDNA), were immobilized on the Au nanodot arrays. Cytochorme c and single stranded DNA could be immobilized on the Au nanodot using the chemical linker 11-MUA and thiol-modification by covalent bonding, respectively. The atomic structure of the fabricated nano-platform device was characterized by scanning electron microscopy (SEM) and atomic force microscopy (AFM). The electrical conductivity of biomolecules immobilized on the Au nanodot arrays was confirmed by scanning tunneling spectroscopy (STS). To investigate the activity of biomolecule-immobilized Au-nano dot array, the cyclic voltammetry was carried out. This proposed nano-platform device, which is composed of biomolecules, can be used for the construction of a novel bioelectronic device.

Delivered by Publishing Technology to: Sung Kyun Kwan University
IP: 115.145.129.86 On: Tue, 18 Jun 2013 08:01:27
Copyright: American Scientific Publishers

Keywords: Au Nanodot, Atomic Force Microscopy, Biomolecule, Bioelectronic Device, Nanobiochip.

1. INTRODUCTION

In recent years, biotechnology has made significant advances in the field of biomaterials and has been able to address several current limitations of biomaterials without the help of other scientific disciplines.[1–4] However, as this field progressed there was an increasing need to understand the behavior of biomaterials at the nanoscale, which could not be addressed without the involvement of other fields of science such as engineering. Hence, early on in the field, a few pioneering groups attempted to better understand the intrinsic properties of biomaterials on the nano-scale by integrating with other scientific areas. The result of this early work was the development of a whole new important area of biotechnology, nanobiotechnology.[5–9] The formation of well-structured nanostructures with high density, well orientation, and uniform sizes is of interest for nanobiotechnology applications such as bioelectronic devices and biosensors. In particular, the nanodot array technique was demonstrated to provide a very stable and well-organized platform for fabricating biomolecules-based sensors or electronic devices. In this regard, various lithographic techniques have been used to produce uniform nanodot arrays including, focused ion beam, ion beam sputtering and electron beam lithography.[10–12] However, these techniques have some limitations such as a high production cost and low efficiency in terms of large area production. Due to these limitations, a self-ordered nanoporous alumina layer composed of a hexagonal lattice pattern has been used as a template to fabricate nanostructured patterns. The Au nanodot structure has some advantage in terms of developing bioelectronic devices in that the binding of biomolecules to Au is relatively simple and well established.[13]

Choi's group has previously developed a bioelectronic device that performed a simple function. For example,

*Authors to whom correspondence should be addressed.

 1533-4880/2013/13/6020/007 doi:10.1166/jnn.2013.7647

they developed a shift register memory device that consisted of biomolecular Langmuir-Blodgett heterofilms that could function as a biomolecular diode and an electrical signal switching device using photons for current generation.[14–15] Also, they developed various bioelectronic devices that consisted of metalloproteins.[16–18] However, these bioelectronic devices were developed in the bulk state. In this study, a bioelectronic device was developed by self-assembling cytochrome c and thiol-modified single strand DNA on a Au nanopattern, which allowed for control over the biomolecules at nanoscale.

Therefore, in this study, we attempted to fabricate a well organized nanostructure for various bioelectronic device applications. Cytochrome c was immobilized on Au dot using the chemical linker 11-MUA. The 11-MUA contained a thiol group on one end of the molecule and carboxyl group on the other end. The thiol group of the 11-MUA was anchored to the Au surface and the carboxyl group of 11-MUA was reacted with the free amine groups of cytochrome c. Thus, cytochrome c was anchored to the Au nanodot via 11-MUA. In contrast, no additional linker was needed for the immobilization of thiol-modified ssDNA, due to presence of the thiol group in terminal structure of ssDNA. Figure 1 shows a schematic diagram of the fabricated nano-platform containing cytochrome c and thiol-modified ssDNA. To confirm successful fabrication of the Au nanopattern, SEM was used to image the surface morphology of the Au nanodot. In addition, the morphology of the Au nanopattern surfaces containing self-assembled biomolecules was investigated by atomic force microscopy (AFM). Finally, the electrical characteristics were analyzed by scanning tunneling spectroscopy (STS).

Delivered by Publishing Technology to: Sung Kyun Kwan University
Copyright American Scientific Publishers

2. EXPERIMENTAL DETAILS

2.1. Materials and Methods

The ITO glass and Au was purchased from G-mek (Korea) and used to make the Au nanodot. Cytochrome c was purchased from Sigma Aldrich Co (USA). A thiol-modified ssDNA (26 mer: 5′-CCCGGGAAACCCGGGTTTAAAAA AAA-3′) and complementary ssDNA (16 mer: 5′-AACC AACCTTTTTTTT-3′) were purchased from Bioneer (Korea). A HEPES (4-(2-hydroxyethyl)-1-piperazine-ethanesulfonic acid) solution was used as the electrolyte buffer and was purchased from Sigma Aldrich Co (USA). A 0.1 mg/ml cytochrome c solution was dissolved in 10 mM HEPES buffer at pH 7.0. A 20 μl solution of 1 μM thiol-modified ssDNA was diluted in DNase free water (Welgene, Korea). Distilled and deionized (DI) water was used to clean the substrates.[19]

2.2. Fabrication of Anodic Aluminum Oxide Mask

A well-ordered anodic aluminum oxide (AAO) was prepared from aluminum foil using the two-step anodization process developed by Masuda.[22] The fabrication process, which utilized a AAO mask, was described in detail elsewhere.[23–24] The first anodization was performed by

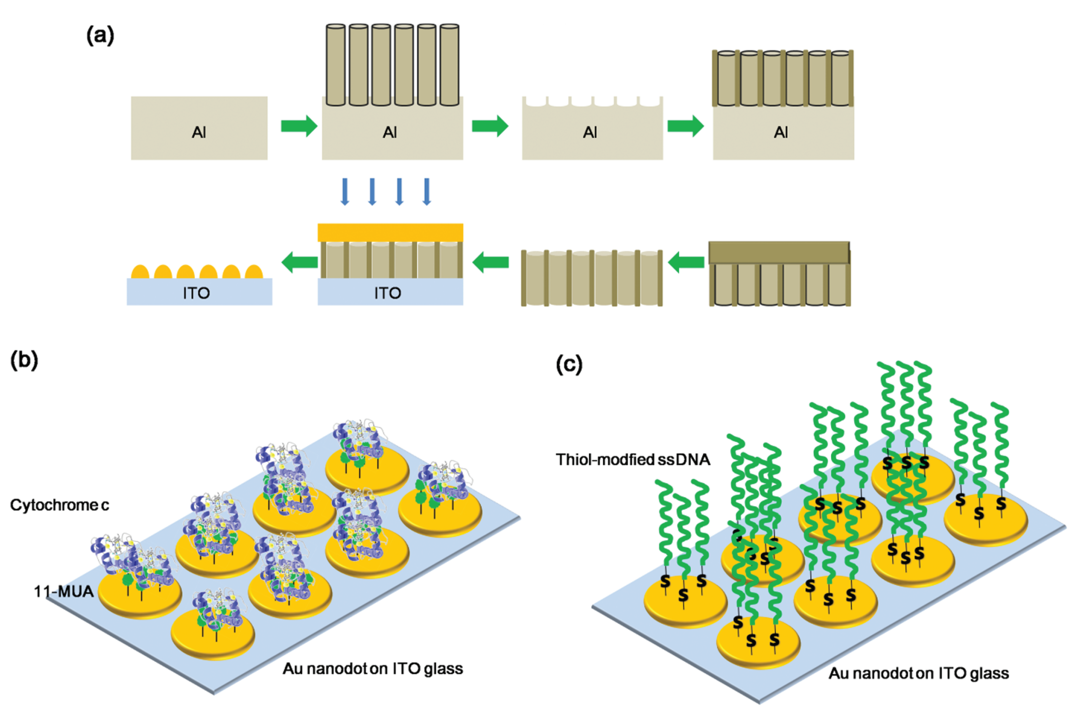

Fig. 1. Schematic representation of (a) the experimental process used for the fabrication of the Au nanodots pattern on ITO glass. (b) Immobilization of cytochrome c self-assembled on Au dot surface via 11-MUA. (c) Immobilization of thiol-modified ssDNA onto Au-nanodots.

RESEARCH ARTICLE

applying a DC voltage of 40 V in a 0.3 M oxalic acid solution at 3 °C for 8 hr. The well-ordered AAO mask was produced by completely removing the alumina layer formed during the first anodization process by chemical wet etching in a mixed solution consisting of phosphoric acid (0.4 M) and chromic acid (0.2 M) at 65 °C for 6 hrs. After removing the alumina layer, the second anodization process was conducted for 4 min under identical conditions used for the first anodization. After the second anodization, a coating layer containing nitrocellulose and polyester resin in butyl acetate, ethyl acetate, and isopropyl alcohol, was painted on the surface of the AAO. The remaining aluminum substrate was removed in a saturated $HgCl_2$ solution. The AAO layer was etched in 5 wt% solution of H_3PO_4 at 30 °C. The coating layer was then dissolved in acetone.

2.3. Fabrication of Au Nanodot Pattern

The AAO mask containing through-holes was placed onto an ITO-coated glass substrate. Au deposition was then carried out by thermal evaporation. After Au deposition, the alumina mask bonded to the ITO substrate was dissolved in 1 M NaOH for several minutes.

2.4. Immobilization of Biomolecules on Au Nanodot

To immobilize cytochrome c onto the Au nanodot, an additional linker molecule, 11-MUA, was needed. 11-MUA was dissolved in 5:5 (ethanol:glycerol) mixture to a final 11-MUA concentration of 5 mM. The 11-MUA solution was then incubated with the Au nanodot surface for 12 hrs at ambient conditions. During the self-assembly process, the thiol group of the 11-MUA molecule should form a covalent bond with the Au dot surface. After this was complete, the modified Au nanodot surface was cleaned with ethanol and DI water to remove excess residues. The cleaned surface was dried using a stream of N_2 gas. 20 ul of the cytochrome c (0.1 mg/ml) solution was then incubated with the self-assembled 11-MUA layer for 6 hrs to allow for protein immoblixation. In this step, a covalent bond should form between the amine groups of cytochrome c and the carboxyl group of 11-MUA. The cytochrome c modified Au nanodot substrates were rinsed with DI water and dried by N_2 gas.

A thiol-modified single strand DNA (26 mer) was also self-assembled on the Au nanodot surface. In this case, self assembly of the thiol-modified ssDNA did not require any additional linker material. Thus, thiol-modified ssDNA was directly immobilized through a covalent bond between the thiol group of the ssDNA and Au. 20 μl of the 1 μM thiol-modified ssDNA solution was incubated with the Au nanodot for 6 hrs. DI water was then used to rinse the immobilized Au surface. And then, the complementary ssDNA (cDNA) was also prepared to determine the hybridization for 3 hrs.

2.5. Topographic Analysis of Biomolecules Immobilized on Au Nanodot by Atomic Force Microscopy

The surface morphology before and after immobilization was investigated by AFM (Digital instruments Nanoscope (R) IV, USA). AFM images were acquired in tapping mode using a Phosphorous (n-type doped Si) tip that had a spring constant of 20–80 N/m a resonant frequency ranging from 230 to 305 kHz. A scan rate of 1.5 Hz was used during imaging.

2.6. Electrical and Electrochemical Property of Biomolecules Self-Assembled on Au Nanodot by Scanning Tunneling Spectroscopy and Cyclic Voltammetry

The scanning tunneling spectroscopy (STS) experiments were conducted using a DI Multimode instrument (Digital instruments, USA). Tungsten (W) tips of 14 mm were used (Veeco instruments, USA) and I–V curves were monitored at tip current/bias voltage of 0.5 nA and 100 mV, respectively. The CV experiment was referred to our previous work.[19,20]

3. RESULTS AND DISCUSSION

Delivered by Publishing Technology to: Sung Kyun Kwan University
IP: 115.145.129.86 On: Tue, 18 ...
Copyright American Scientific Publishers

3.1. Features of Fabricated Anodic Aluminum Oxide (AAO) Mask

Many types of nanostructured materials with a controlled size have been reproducibly fabricated using a self-organized AAO layer. The close-packed hexagonal pore arrays of the AAO plays an important role in determining the ordering and size of the nanostructure. After the second anodization step, the AAO layer thickness was approximately 250 nm. The AAO layer was etched for 26 min in a 5 wt% solution of H_3PO_4 at 30 °C. Figures 2(a) and (b) shows a cross-section SEM image of the AAO mask with through-holes on an ITO-coated glass substrate. The inserted SEM image shows a cross-section SEM image of the AAO mask bonded to the ITO glass. The AAO mask, which had a Ca thickness of 200 nm, was bonded to the ITO substrate via van der Waals forces.[13] The alumina barrier layer at the bottom of the AAO was thoroughly removed by the chemical etching process. The pore diameter of the AAO mask was 60 nm ($\pm$ 5 nm) and the hexagonal cell size was 105 nm. The pore diameter could be adjusted to the range of the hexagonal cell size of the AAO by controlling the dipping time.[24]

3.2. Fabrication of Au Nanodot Pattern

Au was deposited on the ITO-coated glass substrate covered with the AAO mask by thermal evaporation. The slower deposition rate did not block the pores because

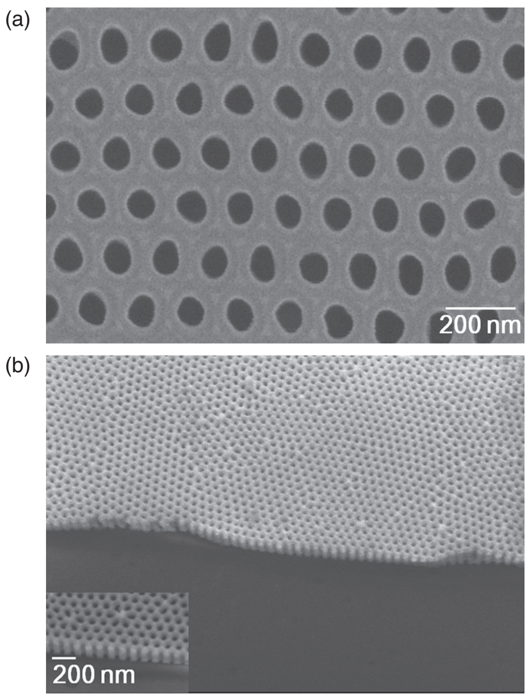

Fig. 2. (a) SEM image of alumina mask/ITO glass before Au deposition. (b) SEM image of the nanoporous alumina mask.

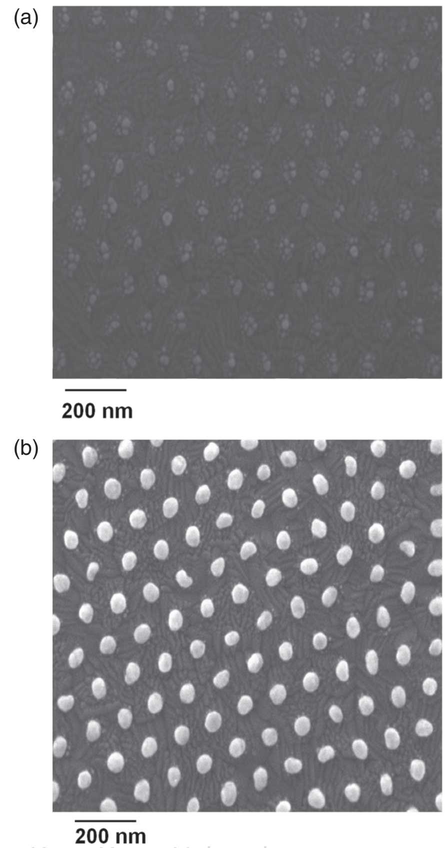

Fig. 3. (a) SEM image of Au deposited alumina mask/ITO glass After Au deposition. (b) SEM image of 60 nm Au nanodots formed on ITO glass after removal of the nanoporous alumina mask.

the AAO mask contained several nanometer-sized holes. Severe deposition of Au on the mask surface can be avoided by controlling the growth rate. A slow growth rate was more effective for the formation of uniform Au dots. The deposition rate used in this study was approximately 0.1~0.2 Å/s. The formation of the Au nanodots also depended on the deposition time. After Au deposition for 100 s, the AAO mask bonded to the substrate was dissolved in a 1 M NaOH solution. After the removal of the aluminum mask, the surface morphology of the Au dots on the ITO substrate was investigated by SEM. After removing the AAO mask, SEM image of the Au nanodot arrays formed on the surface after Au deposition for 2500 s were acquired (Fig. 3(a)). Uniform nanodots in periodic patterns with a mean distance of separation of 105 nm were observed. The average diameter of the nanodots was 60 ± 5 nm. Figure 3(b) shows a SEM image of Au clusters formed on the surface after Au deposition for 500 s. The Au clusters had assembled into a circular shape that was 60 nm in diameter. The nucleation and growth of Au clusters on the substrate below the AAO mask occurred through a process of diffusion accompanied by cluster drift.[14] The AAO mask, which was attached to the substrate, mainly determined the distribution and size of the nanodot arrays.[14] These combined results demonstrate that the Au nano pattern was well fabricated and well structured for the immobilization of biomolecules, which can be used for the development of a bioelectronic device.

Delivered by Publishing Technology to: Sung Kyun Kwan University
Copyright American Scientific Publishers

3.3. Analysis of Fabricated Au Nanodot by AFM and STS, CV

Two separate techniques, AFM and STS, were used to confirm the successful fabrication of the bare Au nanodots. AFM measurements were performed to observe the surface morphology and to check the dot size. Figures 4(a) and (b) show the surface morphology of bare Au at a 400 nm scale. The STS measurement was carried out to analyze the conductive properties of the fabricated Au dot surface. Figure 4(c) describes that the height and width profiles of the Au nanodots formed on ITO surface and which depicts the 61.17 nm size of Au nanodot. In order to compare the efficiency of immobilization effect, the surface coverage (number of biomolecule) and surface roughness of prepared samples were analyzed. The surface roughness (R_a) was estimated from the AFM images analyzing tool. The R_a value was approximately 2.978 ± 0.172 nm for the bare Au surface without any biomolecules. The surface coverage (number of biomolecule) was calculated based on the changes of the surface roughness following each biomolecule immobilization. The coverage was 0. Also, Figure 4(d) shows the surface I–V characteristics of the fabricated Au nanodot as assessed by STS. The I–V plot was acquired by positioning the STM tip on top of the

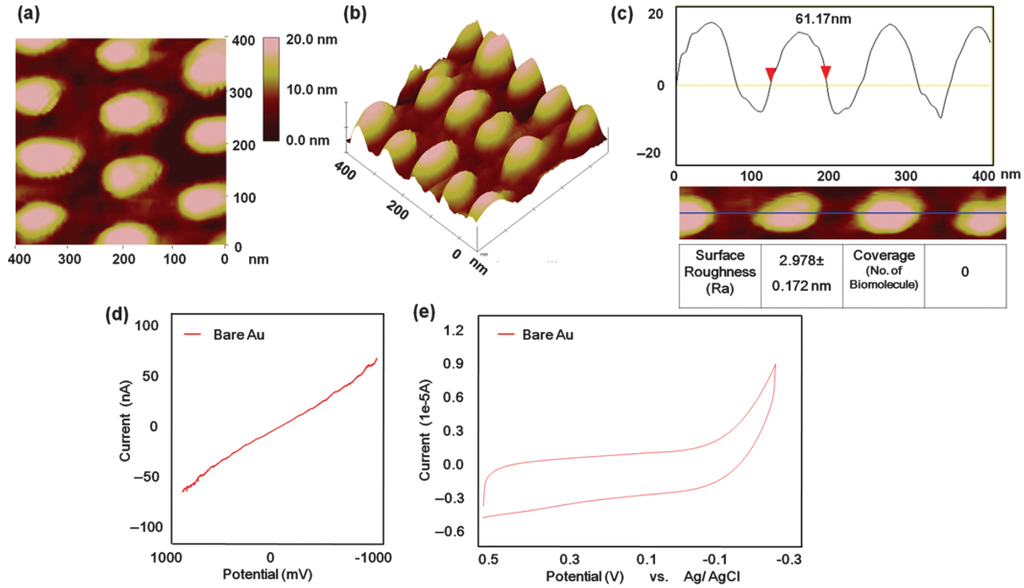

Fig. 4. (a) 2D AFM image of bare Au nanodots. (b) 3D AFM image of bare Au nanodots. (c) The height and width profile of the Au nanodot surface and Surface Roughness, Coverage values of bare Au. (d) STS plot of the surface of the bare Au nanodot engaged at a 500 pA tunneling current and a bias of 0.1 V. (e) Cyclic voltamogram of bare Au nanopattern.

Au dot surface, while the feedback loop was temporarily detached. The tunneling current was then recorded when the sample bias was ramped from −1000 mV to 1000 mV. The *I*–*V* plot had a linear trend with an asymmetric shape. This linearity indicates that the fabricated Au dot was well formed, which will allow for biomaterial immobilization. Moreover, the CV was carried out to determine the activity of biomolecules. In case of bare Au nanopattern, there is no peak observation and the result is shown in Figure 4(e). So, we finally assumed this fabricated Au pattern could be possible to use the bioelectronic device as the platform.

3.4. Analysis of Cytochrome c on Au Nanodot via 11-MUA by AFM and STS, CV

Cytochrome c was immobilized on the Au nanodot via the 11-MUA linker. The protein immobilized Au dot surface was examined by AFM. Figures 5(a) and (b) show AFM images of the cytochrome c/11-MUA layer self-assembled on the Au dots. Based on these images, cytochrome c was determined to be well immobilized on the Au dot surface via 11-MUA. However, lumps of cytochrome c aggregates were also bound to the ITO surface because the 11-MUA molecule can be provide binding sites on the ITO surface due to physical adsorption. The AFM images were taken at a scan size of 400 nm × 400 nm. Figure 5(c) describes that the height and width profiles of the cytochrome c/11-MUA on Au dots surface and which depicts the 5.42 nm size of cytochrome c clusters. The size of cytorhome c was determined approximately 3 nm per one molecule.[19] The surface roughness (R_a) was estimated from the AFM images analyzing tool. The R_a value was approximately 0.743 ± 0.089 and the coverage for each AFM image with programmed software of the instrument gives around the coverage of cytochrome c ($52 < \text{No.} < 72$). Also, The STS experiment was performed to measure the electrical behavior of the cytochrome c molecules on the Au dot. Figure 5(d) depicts the *I*–*V* behavior of cytochrome c/11-MUA on the Au dot surface. The tunneling current was monitored as the sample bias was ramped from −1000 mV to 10000 mV. This feature originated from the interaction between the STM tip and the cytochrome c/11-MUA molecule/conducting surface. Consequently, this asymmetric curve depended on many factors including the conformational change of cytochrome c and length size of 11-MUA. If cytochrome c was directly immobilized on the Au surface, then the current response should have been changed. However, 11-MUA may also act as an insulator, which will depend on the length of the carbon chain. Despite these possibilities, this effect was primarily dominated by the gap between the edge of the tip andcytochrome c surface. As a result, the conductance of the cytochrome c surface showed a different curve compared to bare Au dot. This analysis was conducted at room temperature under normal humidity, which may have also affected the *I*–*V* characteristic of the cytochrome c/11-MUA layer. Presumably, this result can be assumed that two or three cytchrome c molecules formed on Au dot surface. Furthermore, the CV was investigated to monitor the redox property. Figure 5(e) shows the cyclic voltamogram which scan range from 0.5 V to −0.3 V was taken with 0.05 V/s scan rate. The oxidation potential and reduction potential of the cytochrome c was 218 mV and 97 mV, respectively. The formal potential value is 157 mV

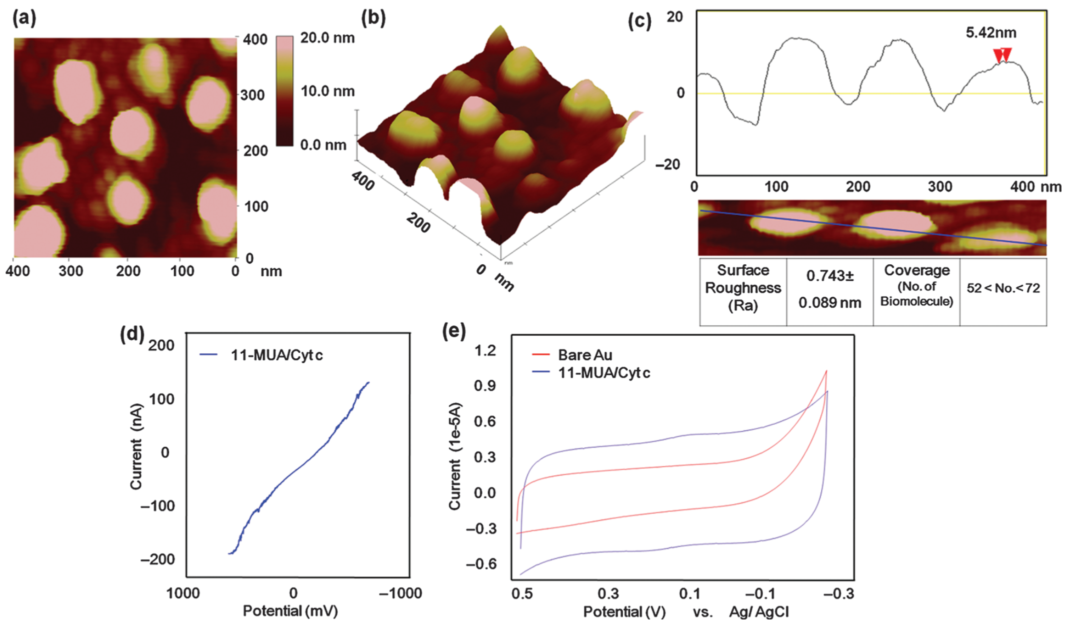

Fig. 5. (a) 2D AFM image of the cytochrome c/11-MUA self-assembled on Au nanodots. (b) 3D AFM image of cytochrome c/11-MUA self-assembled on Au nanodots. (c) The height and width profile of cytochrome c/11-MUA layer surface and Surface Roughness, Coverage values. (d) STS plot of the surface of the cytochrome c/11-MUA self-assembled on Au nanodot engaged at a 500 pA tunneling current and bias of 0.1 V. (e) Cyclic voltamogram of cytochrome c/11-MUA layer (blue line) and bare Au nanopattern (red line).

which having stable potentials. These stable potentials were elucidated from the cyclic voltammogram shows the efficient immobilization of cytochrome c on 11-MUA/Au nanopattern.

IP: 115.145.129.86 On: Tue
Copyright American Scientific Publishers

3.5. Analysis of Thiol-Modified ssDNA on Au Nanodot by AFM and STS

The thiol-modified ssDNA was directly self-assembled on the Au nanodot without the need for a chemical linker. The AFM image of the thiol-modified ssDNA immobilized Au pattern was shown in Figures 6(a) and (b). In the case of thiol-modified ssDNA immobilization, the ssDNA molecules were oriented better compared to cytochrome c/11-MUA. Moreover, Figure 6(c) displays that the height and width profiles of the thiol-modified ssDNA on Au dots surface. The surface analysis data shows the 7.22 nm size of ssDNA moleucles. In case of thiol-modified ssDNA on Au surface, the R_a value is 0.413 ± 0.076 nm and the coverage ($76 <$ No. < 96). This result gave the two

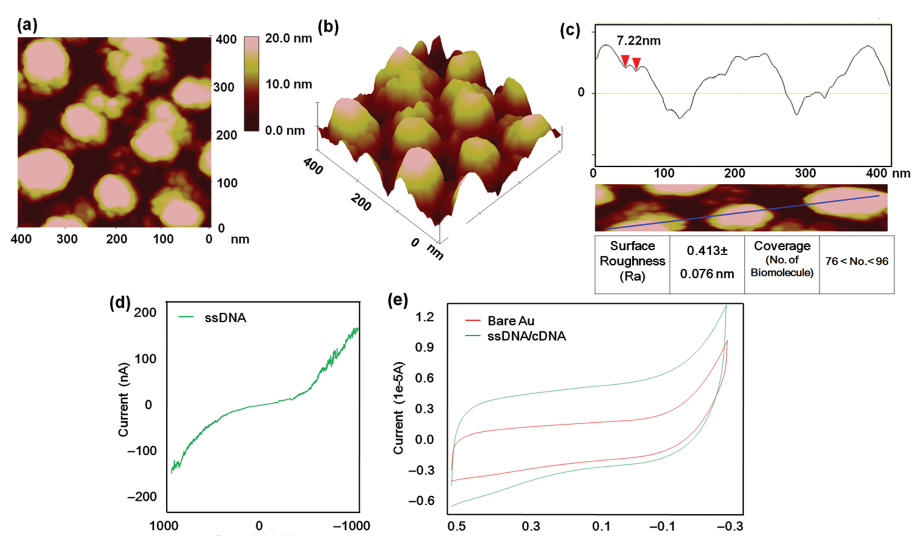

Fig. 6. (a) 2D AFM image of the thiol-modified ssDNA immobilized on Au nanodots. (b) 3D AFM image of the thiol-modified ssDNA immobilized on Au nanodots. (c) The height and width profile of the thiol-modified ssDNA on Au nanodot surface and Surface Roughness, Coverage values. (d) STS plot of the surface of the thiol-modified ssDNA immobilized on Au nanodot engaged at a 500 pA tunneling current and bias of 0.1 V. (e) Cyclic voltamogram of ssDNA/cDNA hybridization (green line) and bare Au nanopattern (red line).

possibility of condition considering ssDNA. First one is the thiol-modified ssDNA aggregates with surrounding DNA molecules. And second one is the thiol-modified ssDNA laid on Au surface by physical adsorption. This result indicates that direct immobilization without a chemical linker is a more effective immobilization strategy. The electrical property of the ssDNA/Au was investigated by recording the I–V response curves. The sampling bias was ramped from −1000 mV to 1000 mV and the current response due to the electrical properties of the ssDNA was monitored. Figure 6(d) shows the STS curve of thiol-modified ssDNA immobilized on the Au nanopattern. The STS plot shows the tunneling current, which was reflected between the external structure of the ssDNA and the edge of the STM tip. This asymmetric current response mainly depended on the STM tip/ssDNA/Au surface. In addition, other factors affected the current response. For example, when an electric field was applied, a conformational change in the ssDNA was triggered. Moreover, the air and humidity conditions may have also affected the current response. Overall, the I–V curve of ssDNA adopted a different shape compared to the bare Au dot or cytochrome c/11-MUA immobilized on the Au dot.

Moreover, the CV was investigated to monitor the redox property of ssDNA/cDNA hybridization. The oxidation potential and reduction potential of the ssDNA/cDNA hybridization was 361 mV and 132 mV and this was shown in Figure 6(e). The formal potential value is 246.5 mV which having stable potentials. These stable redox potentials were elucidated from the cyclic voltammogram shows the efficient hybridization of ssDNA/cDNA on Au nanopattern. Based on these results, we can easily conclude that the thiol-modified ssDNA was well formed, appropriately oriented and retained its original characteristics on the Au dot. In the further study, if we can control the behavior of ssDNA single molecule, we also make the ssDNA bioeletronic device based on single molecule. Consequently, this approach which consisted of ssDNA can be used for the development of bioelectronic devices such as DNA-based biosensors.

Delivered by Publishing Technology to: Sung Kyun Kwan University
IP: 115.145.129.86 On: Tue, 18 Jun 2013 02:01:27
Copyright: American Scientific Publishers

4. CONCLUSIONS

In the present study, biomolecules were successfully self-assembled on the Au nanodot. Using a well-ordered anodic aluminum oxide (AAO) mask, which was prepared from aluminum foil, Au nanodots were fabricated using the thermal evaporation method. In this process, Au nanodots, which were 60 nm in diameter, were formed on an ITO glass substrate to match the ordered nanoporous alumina mask. The fabricated Au nanodots on the ITO glass were confirmed by SEM and AFM. Cytochrome c was immobilized on the Au nanodot by using 11-MUA as a chemical linker. In addition, thiol-modified ssDNA was directly self-assembled on the Au surface. The successful immobilization of these two biomolecules was verified by AFM, STS and CV. The combined results of this study demonstrate that Au nanodots fabricated using the alumina mask can be easily used as a nanoplatform for the development of bioelectronic devices.

Acknowledgments: This research was supported by The Nano/Bio Science and Technology Program (M10536090001-05N3609-00110) of the Ministry of Education, Science and Technology (MEST), the National Research Foundation of Korea (NRF) grant funded by the Korea government (MEST) (2012-0000163), by the project of National Junior research fellowship which National Research Foundation of Korea conducts from 2012.

References and Notes

1. N. C. Seeman, *Nature* 421, 427 **(2003)**.
2. G. Seelig, D. Soloveichik, D. Y. Zhang, and E. Winfree, *Science* 314, 1585 **(2006)**.
3. I. Willner and E. Katz, *Angew. Chem. Int. Ed.* 39, 1180 **(2000)**.
4. S.-W. Lee, C. Mao, C. E. Flynn, and A. M. Belcher, *Science* 296, 892 **(2002)**.
5. C. M. Lieber and W. Lu, *Nat. Mater.* 6, 841 **(2007)**.
6. J. R. Heathand and M. A. Ratner, *Phys. Today* 56, 43 **(2007)**.
7. Z. Liu, A. A. Yasseri, J. S. Lindsay, and D. F. Bocian, *Science* 302, 1543 **(2003)**.
8. J. H. Schon, H. Meng, and Z. Bao, *Science* 294, 2138 **(2001)**.
9. K. M. Roth, A. A. Yasseri, Z. Liu, R. B. Dabke, V. Malinovskii, K. H. Schweikart, L. Yu, H. Tizando, F. Zaera, J. S. Lindsey, W. G. Kuhr, and D. F. Bocian, *J. Am. Chem. Soc.* 125, 505 **(2003)**.
10. R. Gago, L. Vázquez, O. Plantevin, T. H. Metzger, J. Munŏz-Garcia, R. Cuerno, and M. Castro, *Appl. Phys. Lett*. 89, 233101 **(2006)**.
11. V. Corradini, U. D. Pennino, R. Biagi, V. D. Renzi, A. Gambardella, G. C. Gazzadi, A. Candini, L. Zobbi, and A. Cornia, *Surf. Sci.* 601, 2618 **(2006)**.
12. T. H. P. Chang, M. Mankos, K. Y. Lee, and L. P. Muray, *Microelectron. Eng.* 57, 117 **(2000)**.
13. M. Jung, S.-I. Mho, and H. L. Park, *Appl. Phys. Lett*. 88, 133121 **(2006)**.
14. J. W. Choi and M. Fujihara, *Appl. Phys. Lett.* 84, 2187 **(2004)**.
15. Y. S. Nam, J. W. Choi, and W. H. Lee, *Appl. Phys. Lett*. 85, 6275 **(2004)**.
16. J. Min, T. Lee, S.-M. Oh, H. Kim, and J. W. Choi, *Biotechnol. Bioproc. E* 15, 30 **(2010)**.
17. J. W. Choi, J. S. Kim, S. U. Kim, and J. Min, *Biochip J*. 3, 157 **(2009)**.
18. T. Lee, S.-U. Kim, J. Min, and J.-W. Choi, *Adv. Mater.* 22, 510 **(2010)**.
19. H.-Y. Cho, T.-H. Kim, S.-U. Kim, and J.-W. Choi, *J. Nanosci. Nanotechnol*. 12, 834 **(2012)**.
20. S.-M. Kang, T.-H. Kim, and J.-W. Choi, *Nanotechnology* 12, 5185 **(2012)**.
21. H. Masuda and M. Satoh, *Jpn. J. Appl. Phys*. 35, 126 **(1995)**.
22. M. Jung, B.-K. Oh, and J.-W. Choi, *Ultramicroscopy* 109, 1006 **(2009)**.
23. C. Y. Han, G. A. Wiling, Z. Xiao, and H. H. Wang, *Langmuir* 23, 1564 **(2007)**.

Received: 27 July 2012. Accepted: 20 December 2012.